



The sensitivity of atmospheric blocking to changes in upstream latent heating - numerical experiments

Daniel Steinfeld¹, Maxi Boettcher¹, Richard Forbes², and Stephan Pfahl³

¹Institute for Atmospheric and Climate Science, ETH Zürich, Switzerland

²European Centre for Medium-Range Weather Forecasts, Reading, United Kingdom

³Institute of Meteorology, Freie Universität Berlin, Germany

Correspondence: Daniel Steinfeld (daniel.steinfeld@alumni.ethz.ch)

Abstract. Recent climatological studies based on trajectory calculations have pointed to an important role of latent heating during cloud formation for the dynamics of anticyclonic circulation anomalies such as atmospheric blocking. However, the causal relationship between latent heating and blocking formation has not yet been fully elucidated. To explicitly study this causal relationship, we perform sensitivity simulations of five selected blocking events with a global weather prediction model in which we artificially eliminate latent heating in clouds upstream of the blocking anticyclones. This elimination has substantial effects on the upper-tropospheric circulation in all case studies, but there is also significant case-to-case variability: some blocking systems do not develop at all without upstream latent heating, while for others the amplitude of the blocking anticyclones is merely reduced. This strong influence of latent heating on the jet stream is due to the injection of air masses with low potential vorticity (PV) into the upper troposphere in strongly ascending “warm conveyor belt” airstreams, and the interaction of the associated divergent outflow with the upper-level PV structure. The important influence of diabatic heating demonstrated with these experiments suggests that an accurate parameterization of microphysical processes in weather prediction and climate models is crucial for adequately representing blocking dynamics.

Keywords: atmospheric blocking, atmospheric dynamics, jet stream, extratropical cyclone, mid-latitude weather, latent heating, diabatic processes, potential vorticity, numerical sensitivity simulation.

1 Introduction

The formation and maintenance of prolonged anticyclonic circulation anomalies, denoted as atmospheric blocking, represents an important and challenging aspect of mid-latitude weather variability. Atmospheric blocking leads to persistent changes in the large-scale circulation and blocks the westerly flow (Rex, 1950; Woollings et al., 2018), often causing anomalous, sometimes extreme weather (Green, 1977) in a situation of increased forecast uncertainty in weather models (Pelly and Hoskins, 2003; Rodwell et al., 2013).

Despite its importance, there is currently no comprehensive theory of blocking (for a review see Tyrllis and Hoskins, 2008). Several dynamical processes have been identified to be conducive to blocking formation, such as planetary-scale wave dynamics (e.g., Charney and DeVore, 1979; Hoskins and Valdes, 1989; Petoukhov et al., 2013), forcing by transient eddies (e.g., Shutts, 1983; Luo et al., 2014) and Rossby wave breaking (Pelly and Hoskins, 2003; Altenhoff et al., 2008), with evidence



25 that different processes can dominate in different blocking cases (e.g., Nakamura et al., 1997; Drouard and Woollings, 2018; Steinfeld and Pfahl, 2019). Atmospheric blocking occurs when an air mass with anomalously low potential vorticity (PV) is advected poleward, related to a meridionally amplified flow (Nakamura and Huang, 2018), setting up a large-scale negative (anticyclonic) PV anomaly in the upper troposphere at the level of the mid-latitude jet stream and a stable surface anticyclone underneath (Hoskins et al., 1985). Such large-scale advection of anticyclonic air masses into the blocking region occurs typi-
30 cally on the downstream side of developing baroclinic waves (e.g., Colucci, 1985; Mullen, 1987; Nakamura and Wallace, 1993; Yamazaki and Itoh, 2012), which is the synoptic mechanism behind the classical 'eddy-mean flow' view, i.e. the dynamical interaction between synoptic transient eddies and the large-scale flow (e.g., Berggren et al., 1949; Green, 1977; Shutts, 1983; Hoskins et al., 1983).

While these concepts focused on dry-adiabatic mechanisms, recent climatological studies based on trajectory calculations using reanalysis data (Pfahl et al., 2015; Quinting and Reeder, 2017; Steinfeld and Pfahl, 2019) demonstrated that moist-diabatic
35 processes, and in particular latent heating (LH) during cloud formation in strongly ascending airstreams, play a significant role for the dynamics of blocking. The primary effect of latent heat release on blocking is the diabatic generation and amplification of upper-level negative PV anomalies (Pfahl et al., 2015). This amplification results from the injection of low PV into the upper troposphere in cross-isentropic ascending airstreams and the interaction of the diabatically enhanced divergent outflow with
40 the upper-level PV structure at the tropopause (Steinfeld and Pfahl, 2019). For example, these diagnostic studies have shown that LH occurs predominantly in the warm conveyor belt (WCB) of extratropical cyclones and is generally most important during blocking onset and in more intense and larger blocks. In addition, the repeated injection of diabatically heated low-PV air during the blocking life cycle, associated with a series of transient cyclones approaching the block, can act to maintain blocks against dissipation. These findings complement the large body of previous work that found LH to be important for the
45 development of mid-latitude weather systems, such as cyclones (Ahmadi-Givi et al., 2004; Binder et al., 2016), Rossby waves (Grams et al., 2011) and Rossby wave breaking (Zhang and Wang, 2018).

Nevertheless, as these previous studies have used diagnostic methods to determine statistical relationships between LH and blocking, the causal effect of LH on blocking, and for the wave dynamics at the tropopause in general, is still not completely understood. It is a challenge to quantify this impact of LH, mainly because LH is strongly coupled to the dry dynamics of
50 baroclinic waves and the associated adiabatic advection of PV (e.g., Kuo et al., 1990; Teubler and Riemer, 2016). The question of whether LH critically modifies the development of blocking, that is otherwise mostly affected by dry dynamics, and the investigation of the corresponding cause-and-effect relationship is the focus of this study.

The main objective of this paper is to study the sensitivity of atmospheric blocking to changes in upstream LH in numerical model simulations. The effects of LH on the development (onset, maintenance and decay) of five different blocking events
55 are studied in detailed sensitivity experiments, in which cloud-related LH is altered in the storm track region upstream of the block. In doing so, changes in the formation and maintenance of blocking in these simulations can be attributed to altered LH upstream.



The sensitivity experiments are presented as follows. Section 2 describes the methodology, while section 3 exemplarily introduces one blocking event with a synoptic overview. The results of the sensitivity experiments are presented in section 4 and our conclusions are summarized and discussed in section 5.

2 Methods

2.1 Model setup

This work is based on numerical simulations with ECMWF's global Integrated Forecast System (IFS) cycle 43R1, which was operational between November 2016 and July 2017. The model is run at a cubic spectral truncation of TC0319, which corresponds to roughly 32 km grid spacing, and with 91 vertical levels. ECMWF operational analysis fields are used for initial conditions. 3-hourly output fields, including physical temperature tendencies, are interpolated to a regular grid at 1° horizontal resolution.

In the IFS sub-grid scale processes are represented by various parametrization schemes (ECMWF, 2016). The cloud and large-scale precipitation microphysics scheme, based on Tiedtke (1993), includes five prognostic variables (cloud fraction, cloud liquid water, cloud ice, rain and snow) with associated sources and sinks (Forbes et al., 2011; Ahlgrimm and Forbes, 2013; Forbes and Ahlgrimm, 2014). Convection is parametrized according to Tiedtke (1989) and Bechtold et al. (2008), with a modified CAPE closure (Bechtold et al., 2013).

2.2 Sensitivity experiments

Following a series of seminal numerical sensitivity studies that investigated the role of LH in cyclone dynamics (e.g., Kuo et al., 1990; Stoelinga, 1996; Büeler and Pfahl, 2017), the total effect of cloud-diabatic heating on atmospheric blocking is investigated with sensitivity experiments by comparing the full-physics control simulation including LH (hereafter referred to as CNTRL) to the corresponding simulation without LH (NOLH). LH is artificially turned off by multiplying the instantaneous temperature tendencies due to parameterized cloud and convection processes with a factor $\alpha = 0.0$, but still allowing for moisture changes due to cloud and precipitation formation. Other non-conservative processes, such as radiative heating and turbulent mixing, which can also modify PV (Spreitzer et al., 2019; Attinger et al., 2019), are not altered. In contrast to previous studies, here LH is only modified in the region that is identified to be directly relevant for the blocking system, which is typically the WCB ascent region associated with upstream extratropical cyclones (Steinfeld and Pfahl, 2019). In doing so, we can attribute the changes in the structure of the blocking in these simulations to the altered LH in the confined upstream region, while allowing for heating/cooling everywhere else in the global domain. Our experiment aims to suppress strongly ascending airstreams like WCBs that lead to a strong divergent outflow and PV modification during ascent. Heating along the WCB by cloud microphysical processes is strongest in the lower and middle troposphere (Joos and Wernli, 2012). In order to isolate the effect of this LH, a 3-dimensional box is placed over the main heating region, and LH is only modified in this box. The box has a vertical extent between 900 - 500 hPa and a horizontal extent which is adjusted for each blocking case (see Table



1). To define the heating region objectively, location and time of strongest latent heat release are determined along backward
90 trajectories initiated in the upper-tropospheric blocking in the CNTRL simulation (cf. Steinfeld and Pfahl, 2019). It should be
kept in mind that other microphysical processes, such as ice-phase microphysics close to the outflow level, can also contribute
to the heating and PV modification along the WCB (Joos and Wernli, 2012). As these processes also occur above 500 hPa, our
approach does not fully remove all cloud-related LH, and there is still moderate heating/cooling outside of the box. Near the
edges of the box (in a zone of 5° horizontally and 50 hPa in the vertical), the temperature tendency multiplying factor α is
95 interpolated linearly to obtain a smooth transition from $\alpha = 0.0$ to 1.0.

The sensitivity experiments are performed for five selected case studies of blocking events (see Table 1). The simulations
are run for 10 days. The initialization time is selected such that the observed blocking is adequately simulated in the CNTRL
simulation, as verified visually against ECMWF analysis. For all cases, the simulations are initialized during the intensification
phase of an upstream cyclone, which is typically between 2-3 days prior to blocking onset. The blocking decay is not always
100 captured in the 10-day simulations, as many blocks persisted longer.

LH in extratropical cyclones is coupled to and interacts with other processes, and hence, its artificial removal can affect many
aspects of the flow, such as the cyclone intensification and its baroclinic coupling to the upper-level trough (e.g. Hoskins et al.,
1985). The role of LH in explosively developing cyclones has been studied in great detail, and thus, we focus on the evolution
and structure of upper-level blocking here. However, to better understand such non-linear interactions and their effect on the
105 large-scale flow, we additionally conduct sensitivity experiments with reduced LH ($\alpha = 0.5$) and increased LH ($\alpha = 1.5$) for
one specific blocking event.

2.3 Diagnostic methods

A combination of Eulerian and Lagrangian diagnostics is applied to study the processes involved in the development of block-
ing, and in particular the role of latent heat release in ascending airstreams. The term “upper-level” is used hereafter to describe
110 the vertically averaged flow between 500 and 150 hPa.

2.3.1 Atmospheric blocking tracking

Following Schierz et al. (2004a), blocking is identified and tracked as upper-level negative PV anomalies. The anomalies
are calculated with respect to the calendar-month averages over the ERA-Interim reanalysis period 1979–2016 (Dee et al.,
2011) and temporally smoothed with a 2-day running mean filter. Different thresholds for intensity, persistence and quasi-
115 stationary have been tested in order to track and compare upper-level negative PV anomalies in both CNTRL and NOLH
simulations. In all simulations, blocks are identified with a threshold of -1 pvu and a spatial overlap of 80 % between two
consecutive time steps. No persistence criterion is applied. The reason for this is that the tracked negative PV anomalies in the
NOLH simulations are weak (see below) and would not be classified as persistent blocks (see also Croci-Maspoli et al., 2007).
Nevertheless, all blocking events investigated here also fulfill the stricter blocking criteria used, e.g., by Steinfeld and Pfahl
120 (2019) in the CNTRL simulation. The advantage of the PV-anomaly-based (APV) index is that it objectively captures the core
of the anomalous anticyclonic circulation and thus directly allows for an investigation of the origin and evolution of individual



blocks and the associated air masses. A number of relevant blocking characteristics and their evolution are calculated during the blocking life cycle, such as location (center of mass) and track, spatial extent, blocking intensity (area-averaged upper-level negative PV anomaly) and lifetime. The calculated quantities are area-weighted with the cosine of latitude.

125 2.3.2 Effects of latent heating

To capture the full three-dimensional complexity of LH in ascending airstreams and to quantify its effect on blocking dynamics, a combined Eulerian and Lagrangian perspective is adapted. The effects of LH on the upper-tropospheric PV distribution are quantified as follows:

- **Backward trajectories:** To estimate the relative contributions of dry (adiabatic transport of mass) and moist (cross-
130 isentropic transport of mass) processes to upper-level negative PV anomalies that characterize blocking, we compute kinematic 3-day backward air-parcel trajectories based on the three-dimensional wind using the Lagrangian Analysis tool LAGRANTO (Wernli and Davies, 1997; Sprenger and Wernli, 2015). The trajectories are started from an equidistant grid ($\Delta x = 100$ km horizontally and $\Delta p = 50$ hPa vertically between 500 and 150 hPa) in a blocking region every three hours, with the additional criterion that PV must be smaller than 1 pvu to exclude points located in the stratosphere. Since
135 both PV and potential temperature θ are conserved for adiabatic and frictionless motion, changes in these variables between two time steps along a trajectory are attributed to diabatic processes, such as cloud formation, radiation and friction. Following the method of Pfahl et al. (2015) and Steinfeld and Pfahl (2019), the effect of LH is quantified by the percentage of blocking trajectories with a maximum heating (Lagrangian change of θ) of $\Delta\theta > 2$ K during the three days prior to reaching the blocking region (in the following denoted as LH contribution).
140 considered as an indirect diabatic impact.
- **PV advection:** Considered as an indirect diabatic effect of LH (Davis et al., 1993), the effect of the divergent outflow on the structure and development of blocking is evaluated here by calculating the PV advection by the divergent (irrotational) component ($\mathbf{v}_\chi \cdot \nabla PV$) of the full wind following Riemer et al. (2008) and Archambault et al. (2013). The divergent wind is obtained via Helmholtz partitioning, using a successive overrelaxation method. In addition, the role of the rotational
145 (non-divergent) wind component (\mathbf{v}_ψ) is investigated, which highlights the contribution of the balanced flow associated with the upper-level PV distribution. PV advection by the divergent and rotational wind is averaged vertically between 500 - 150 hPa.

2.4 Overview of the cases

150 Atmospheric blocking covers a variety of flow patterns, including Ω -shaped or high-over-low dipole blocks, which can occur all year round in different regions (Woollings et al., 2018). Important factors for the importance of LH in blocking are the presence of an upstream cyclone and the availability of moisture, which is reflected in a large case-to-case and spatial variability of the LH contribution to blocking (Steinfeld and Pfahl, 2019). The median LH contribution for 4270 blocks in the global ERA-Interim climatology is around 45 %, ranging from 0 % up to over 80 % for individual cases (Steinfeld and Pfahl, 2019).



To cover part of this variability we perform sensitivity experiments for five different blocking events, which develop under
155 different environmental conditions (different seasons, geographical locations and LH contribution), as summarized in Table 1.
Blocks are selected from the main blocking regions over the North Atlantic and North Pacific, but also from a secondary region
over Russia. Some of those blocks are associated with extreme weather events: the 2010 summer heat wave in western Russia,
the devastating wildfires in Canada in May 2016 and the cold spell in Europe in February 2018. The cases “Thor onset” and
“Canada” show a median LH contribution of around 50 %, and “Thor maintenance”, “Cold spell” and “Russia” show a weaker
160 LH contribution.

One of these cases, Thor (onset and maintenance) in the year 2016, is used hereafter to introduce our method. Therefore, its
evolution is described in detail in the following section.

3 Case Study: Block Thor

Block “Thor” occurred over the North Atlantic and Europe in the period 2–19 October 2016, during the North Atlantic Wave-
165 uide and Downstream Impact Experiment (NAWDEX; Schäfler et al., 2018). The onset of Thor was associated with large
forecast uncertainty, in particular the predictability of the upstream cyclone and its diabatic outflow was low (Maddison et al.,
2019). As the block persisted for more than 2 weeks, two simulations are performed here capturing the onset (Thor onset:
30 Sep–10 Oct) and the maintenance/decay (Thor maintenance: 10 Oct–20 Oct) phases. Note that only the second period
was named “Thor” in Schäfler et al. (2018), and the first period was referred to as Scandinavian blocking. However, from a
170 “PV-anomaly” perspective, the entire episode can be described as one persistent blocking event.

The synoptic-scale evolution and several mesoscale features such as the WCB are well predicted by the IFS CNTRL simu-
lations, which can be quantitatively confirmed through comparison with observed cloud top pressure from MSG satellite mea-
surements (Fig. 1). It is evident from Fig. 1a that during blocking onset, a North Atlantic cyclone [named Stalactite cyclone
in Schäfler et al. (2018)] is associated with an elongated band of high-reaching clouds along the cold front and an upper-level
175 trough that wraps cyclonically around the surface low. The outflow of this ascending and cloud-producing airstream concurs
with a strong poleward displacement of the upper-level PV contours. This ridge building marks the onset of block Thor. Ten
days later, Fig. 1b shows the maintenance phase of block Thor, which is characterized by a region of low PV, high surface
pressure and subsidence with low or no clouds over Scandinavia, and two cyclonic systems with high clouds over the North
Atlantic.

180 3.1 Synoptic overview

The life cycle of Thor is characterized by a succession of multiple upstream triggers over the North Atlantic, i.e. synoptic-scale
baroclinic waves, their dynamic interaction with the jet stream and the subsequent formation and maintenance of a downstream
blocking anticyclone. Fig. 2 shows the temporal evolution of the LH contribution, mean diabatic heating along blocking air
masses, blocking intensity and spatial extent for Thor in the two CNTRL simulations (onset and maintenance), and Figs. 3a,c



185 and 4a,b display aspects of the block's evolution at upper levels. On the basis of the APV index, block Thor is tracked from 2–9 October (onset simulation) and 11–19 October (maintenance simulation).

Thor shows typically observed blocking characteristics (e.g., Dole, 1986), such as the rapid onset (fast increase in intensity and spatial extent, Fig. 2) on time scales consistent with synoptic-scale phenomena (2–4 October) and the fluctuation in intensity and size during the blocking lifetime (mature phase: 5–17 October) until its decay (19 October). The episodic nature
190 of the LH contribution and the mean diabatic heating confirm that the importance of LH changes throughout the life cycle, alternating between times when either moist-diabatic (heating) processes or quasi-adiabatic (cooling) processes dominate: the LH contribution is generally largest during onset (70 %) and then declines to the lowest value (almost 0 %) when the block decays. However, there are multiple bursts of LH (local maxima of LH) during the life cycle, which are followed by fluctuations in intensity and size. The block exhibits its most rapid amplification during such LH bursts, suggesting that there is a linkage
195 between moist-diabatic processes and the development of the block. Averaged over the entire lifetime (onset and maintenance), Thor has a LH contribution of 41 %, that is almost half of the blocking air masses have been diabatically heated by more than 2 K.

This episodic nature of LH emphasizes that a series of upstream transient cyclones, rather than a single primary cyclone, contribute to block formation and maintenance. In this case, the upstream triggers (in total 5) include a rapidly intensifying
200 cyclone ahead of an upper-level PV trough (labeled T1 in Fig. 3a), which initiates downstream ridge building R1 and the subsequent onset of the block on 2 October 2016. This is followed by a rapidly propagating surface cyclone T2 from the southwest along an intense baroclinic zone with strong poleward transport of low-PV air in ridge R2, which further intensifies and expands the initial blocking ridge formed by R1 and finally leads to anticyclonic wave breaking and the establishment of a stationary dipole block over Europe (Fig. 3c), resembling the classic dipole blocking structure described by Berggren et al.
205 (1949) and Rex (1950). Maximum intensity of the simulated blocking in terms of upper-level negative PV anomaly and spatial extent occurs around 8 October (8 days into the Thor onset simulation). The block stays well established and stationary for the next days, as the dipolar configuration with a low-over-high PV (or high-over-low geopotential height) anomaly generates an easterly flow at the latitude of the jet (60°N), which counters the advection by the background westerly flow. This is also the time when absolute reversal blocking indices (e.g., following Scherrer et al., 2006), identify the block (not shown).

210 During this mature phase (Fig. 4), which extends into the maintenance simulation, the block is associated with a barotropic signature with a surface high pressure system and a tropospheric-deep anticyclonic flow, splitting the jet stream into northern and southern branches, as indicated by the Z500 contours in Fig. 4a. The deformation region on the western side of Thor leads to the formation of a meridionally-elongated PV filament T3 associated with a small surface cyclone and poleward transport of low-PV air along its eastern flank in ridge R3. T3 is stretched meridionally between block Thor (R2) and a quickly
215 amplifying ridge R4 to the west (Fig. 4a). R4, associated with the intense divergent outflow from an ex-tropical cyclone T4 over the east coast of North America, extends rapidly and replaces R2, thus maintaining a strong and large negative PV anomaly over Northern Europe, contributing to the blocks' persistence. There is a last absorption of low-PV air in migratory ridge R5 before Thor finally decays (Fig. 4c). For this particular event, lysis is a comparatively slow process and is characterized by a synchronous decrease in the intensity and spatial extent while the block slowly moves southeastward.



220 The trajectory analysis in Fig. 5 illustrates the origins and flow history of low-PV air in the blocking anticyclone. Shown are
backward trajectories emanating from the block during onset (Fig. 5a) and maintenance (Fig. 5c). It reveals two distinct types of
airstreams: The first type consists of upper-level trajectories that either (i) originate from the west and flow quasi-horizontally
(and quasi-adiabatically) along the upper-level jet (around the upstream trough) into the block (most evident during onset)
or (ii) are already located in the blocking region at day -3 and recirculate anticyclonically within the block (evident during
225 maintenance). The second type consists of trajectories that ascend rapidly from low levels (> 800 hPa) to higher levels (< 500 hPa)
ahead of surface cyclones over the North Atlantic. Many of these ascending trajectories fulfil the WCB criterion of
600 hPa ascent in 48 hours (Madonna et al., 2014), are heated by ~ 10 K in the median and reach the upper troposphere with
very low PV values (< 0.3 pvu), which corresponds to substantial negative PV anomalies (of roughly -1 pvu in the median).
This ascent occurs primarily on the western flank of the block in regions of strong cloud activity (see again Fig. 1), intense latent
230 heat release and upper-level divergent outflow (Fig. 3a,c,e,g). The divergent wind vectors and LH suggest that the divergent
outflow above the strong heating region contributes to the horizontal rearrangement of upper-level PV.

4 Sensitivity experiments

This section presents the key differences between blocks in the NOLH with respect to the CNTRL simulations focusing on
blocking structure, intensity and evolution. The analysis is restricted to changes in the mid-to-upper troposphere that are most
235 relevant for the evolution of blocking (Hoskins et al., 1985).

We first provide a synoptic comparison between CNTRL and NOLH for Thor onset and maintenance, which helps illustrating
the sensitivity experiments. Synoptic comparison of the other blocking cases can be found in the supplement (Figures S1, S2
and S3).

4.1 Thor: Synoptic differences with and without LH

240 Backward trajectories from Thor identify the North Atlantic storm track as the relevant diabatic heating region (Fig. 5a,c).
Across much of the basin the heating (gray contours in Fig. 3a,c,e,g) occurs in the warm sector of traveling cyclones. Therefore,
the NOLH box is placed over $[60^\circ\text{W} - 0^\circ, 35^\circ\text{N} - 65^\circ\text{N}]$, covering the entire North Atlantic basin, as indicated in the right
panels of Fig. 3 and 4.

It is evident from the backward trajectories shown in Fig. 5b,d that no strongly ascending air masses contribute to the ridge
245 amplification in the NOLH simulations. During blocking onset (Fig. 5b), mostly quasi-adiabatic and quasi-horizontal flow
is associated with Thor. In the maintenance simulation, which is initialized with a mature dipole block (Fig. 5d), the block
is associated with quasi-adiabatic upper-level trajectories that recirculate anticyclonically within the blocking anticyclone,
without the ascending airstreams linked to troughs T3 and T4. Turning off LH over the North Atlantic thus effectively reduces
cross-isentropic transport, and reduces the average LH contribution from 41% (CNTRL) to 16.5% (NOLH). Note that the
250 remaining heated trajectories in NOLH experience considerably less heating (median of ~ 2 K compared to ~ 10 K in CNTRL),
most likely due to ice microphysical process (e.g., depositional growth of snow and ice, see Joos and Wernli, 2012) at higher



altitudes above the NOLH box (cf. method section). Overall, the non-heated trajectories in NOLH show a similar behavior as in the CNTRL simulations.

Given the changes in LH contribution and diabatic heating along the blocking trajectories, we now focus on the impact of LH on the upper-level synoptic-scale flow evolution of Thor. Fig. 3 and 4 compares upper-level PV, Z500, upper-level divergent wind and mid-level cloud-diabatic heating from the NOLH to the corresponding results from the CNTRL simulations. Note that the differences between CNTRL and NOLH are initially weak (after 2 days in the Thor onset and Thor maintenance simulations), but become more pronounced with lead time. Nevertheless, these initial time steps highlight the critical phase when the two simulations start to deviate.

4.1.1 Thor onset

After 2 days, shortly before the block in the CNTRL simulation is identified, remarkable difference in the upper-level PV between the CNTRL (Fig. 3a) and NOLH (Fig. 3b) simulations emerge in the region of ridge R1, with the largest differences in the dynamically active regions associated with the latent heat release and outflow of the heated trajectories. A trough-ridge pattern evolves also in NOLH due to dry baroclinic development of T1, but, in the absence of LH, the amplitudes of the upper-level PV ridges and troughs, as well as the intensity of the upstream cyclone (see SLP contours in Fig. 5a,b) are clearly reduced. This leads to a delayed onset of the block in NOLH compared to CNTRL by one day.

Differences in the upper-level divergent wind are substantial, indicating that diabatic heating significantly enhances the vertical motion and divergent outflow. Moist dynamics account for roughly two thirds of the divergent outflow, which exceeds 10 m s^{-1} in CNTRL compared to $< 3 \text{ m s}^{-1}$ in NOLH. In the CNTRL simulation, a comma-shaped diabatic heating pattern is co-located with the cold front and divergent outflow, which compares favorably with the cloud patterns in the satellite observations (Fig. 1a). The divergent wind above the cloud-diabatic heating maximum in CNTRL aids the westward expansion of ridge R1 through the westward advection of air masses with low PV, shifting the jet stream in the same direction and considerably strengthening the PV gradient. This is also evident from large differences between CNTRL and NOLH in the PV advection by the divergent wind and differences in the upper-level rotational wind in the same region (Supplement Fig. S4a,b), highlighting the role of LH in the amplification and quasi-stationary behavior of blocking. The combined effect of a strong divergent outflow and a meridional amplified rotational flow in CNTRL promotes the growth of the ridge and cyclonic wrap up of high- and low-PV in the upstream trough T1 (Supplement Fig. S4c), suggesting that this cyclonic wave breaking depends essentially on intense LH, since it does not occur in NOLH.

Further into the model integration on day 6 (Fig. 3c,d), the differences between CNTRL and NOLH are considerably more pronounced and it is clear that the large-scale flow develops substantially differently without LH. With the contribution of LH in CNTRL, ridge R2 rapidly amplifies and low-PV air is transported a long way poleward, causing (i) a south-westward extension of the initial blocking region and (ii) a reinforcement of the anticyclonic anomaly formed by ridge R1. The jet stream splits over central Europe with an accelerated southwest - northeast tilted northern branch. When LH is turned off, however, the ascent and outflow are significantly reduced and ridge R2 does not amplify. Instead, R2 is deflected eastward by the westerly winds. As a consequence, the low-PV region of R1 is cut off from the tropospheric reservoir and a zonally oriented jet stream



establishes over western Europe. Without LH, PV values inside R1 are higher, resulting in a less pronounced anticyclonic flow over Europe, as also evident from the Z500 contours. The upper-level synoptic features in NOLH are displaced further downstream, where the flow still splits with a weaker northern branch compared to CNTRL.

4.1.2 Thor maintenance

290 To better understand the role of LH for the persistence of a blocking, we now focus on the Thor maintenance simulation. Both CNTRL and NOLH simulations start with a well established dipole block and a large-scale deformation flow field over Europe, where a large region with low upper-level PV values covers most of Scandinavia on day 2 (Fig. 4a,b). However, first pronounced differences in the divergent outflow strength and the upper-level PV structure occur in the region of upstream ridge R4 to the east of trough T4. In the absence of LH, ridge R4 and consequently the PV streamer T3 are not as strongly
295 extended in the meridional direction as they are in CNTRL, despite being subject to a strong diffluent flow, suggesting that the (dry) eddy straining mechanism (Shutts, 1983) does not fully explain the amplification of the incoming upstream waves. As a consequence, R4 in NOLH does not replace the initial negative PV anomaly R2 over Scandinavia (cf. Fig. 4c,d). Without the contribution of 'fresh' low-PV air, and facilitated by the radiative decay (cooling along upper-level trajectories) of the remaining air masses recirculating inside the block (Fig. 5d), Thor weakens in the NOLH simulation and is no longer captured
300 by the APV blocking index on 15 October (day 5). In contrast, the CNTRL block persists for another 4 days, also due to the additional absorption of anticyclonic air masses in R5 on day 6 (Fig. 3c,d).

4.1.3 Non-linear effects of latent heating

In order to exemplify the non-linearity of the relationship between LH and blocking, Fig. 6 shows the 2 pvu tropopause at day 2 and day 6 of Thor onset with and without LH, and also with reduced LH ($\alpha = 0.5$) and increased LH ($\alpha = 1.5$). The
305 evolution of the tropopause shows a crucial sensitivity to changes in LH with a non-monotonic behaviour of blocking to LH. Note that the modifications of LH first become apparent in the region of the NOLH box over the North Atlantic and only spread out at longer lead times. During the onset phase (day 2, Fig. 6a), the ridge has a larger amplitude and extends further to the west with increasing LH, with cyclonic wrap up of high- and low-PV in the upstream trough most evident in the simulation with enhanced LH ($\alpha = 1.5$, red contour). Consequently, also the downstream trough is more amplified and narrows into a PV
310 streamer in the simulations with unchanged (CNTRL) and enhanced LH. During the mature phase (day 6, Fig. 6b), LH ($\alpha = 1$ and $\alpha = 1.5$) leads to anticyclonic wave breaking and the formation of a stationary dipolar flow pattern that generates strong easterlies at the latitude of the jet over Europe. In addition, the eastward propagation of the upstream trough is slowed down. When LH is reduced or switched off, the ascent and outflow are reduced (not shown), the ridge does not amplify as strongly and, in the absence of wave breaking, blocking is not initiated.

315 The comparison of block Thor with and without LH reveals some interesting differences and helps understanding the causal relationship between LH and blocking during the initiation and maintenance/decay phases. This example illustrates how LH in ascending airstreams embedded in upstream cyclones can play a crucial role in the initiation, but also in the maintenance of blocking, contributing to a more rapid development and longer lifetime of the block. Moist-diabatic processes provide further



flow amplification in addition to dry-dynamical forcing, and repeated LH bursts can extend the lifetime of a block and diminish
320 the tendency for dissipation.

4.2 Set of blocks: Differences with and without LH

To evaluate the sensitivity experiments in a more robust and systematic way, we analyze a set of 5 historical blocks in total
over different regions and in different seasons (see again Table 1).

4.2.1 Differences in upper-level PV structure

325 Figure 7 shows the differences in the upper-level PV and upper-level divergent wind between the NOLH and CNTRL simula-
tions (CNTRL - NOLH) during onset at day 3 for the five blocking cases. In all cases, the dynamical tropopause (2 pvu contour)
is displaced much farther to the pole and west in the regions associated with the divergent outflow in the CNTRL simulations,
along with pronounced differences in the upper-level PV between the CNTRL and NOLH. The absence of LH results in higher
PV and thus in weaker anticyclonic anomalies in NOLH, which is reflected in negative PV differences of more than -1 pvu
330 between CNTRL and NOLH. Because all simulations exhibit similar displacements of the tropopause, it becomes evident that
strong LH embedded in the upstream cyclone is crucial for this initial ridge amplification and the onset of the blocks. The most
pronounced PV differences are co-located with the tropopause, i.e., the region of enhanced PV gradient, which has important
implications for the propagation of Rossby waves in the upper troposphere (Schwierz et al., 2004b; Martius et al., 2010). The
more pronounced ridge also results in a more amplified downstream flow pattern in CNTRL, with the downstream trough
335 penetrating further equatorward.

Differences in the upper-level divergent wind between CNTRL and NOLH are substantial in all cases (more than 5 m s^{-1} ,
see wind vectors in Fig. 7), and it is clear that strong vertical motion (not shown) and upper-level divergence arise from LH.
At these time steps, the divergent wind exceeds 10 m s^{-1} in all CNTRL simulations near the western flank of the ridges and
tends to facilitate its westward and poleward expansion by advecting low PV in these directions. The divergent diabatic outflow
340 substantially contributes to the pronounced upper-level PV differences along the western flank of the ridges through this effect
(see again Figure S4 in the supplement). In the center of the ridges, where PV gradients are weak, PV differences primarily
result from net diabatic injection of low PV air from the lower troposphere in ascending airstreams.

A few days later during the mature phase (6 days into the simulations), Fig. 8 shows substantial differences in the upper-level
PV and upper-level rotational wind between the CNTRL and NOLH simulations. The initial PV differences confined to the
345 north-western flank of the ridges during onset have amplified and propagated up- and downstream, leading to distinctively
different evolution of the upper-level flow with strongly displaced ridges and troughs. In all cases, the intensity and spatial
extent of the blocks are reduced in NOLH, which is reflected in negative PV differences between CNTRL and NOLH. Largest
differences ($\Delta \text{PV} < -3 \text{ pvu}$) are found inside the blocking region, especially in the core (Thor onset, Thor maintenance, Canada
and Russia) and around the flanks of the block (Cold spell). Large PV differences are also found along the upstream and
350 downstream troughs and resemble a dipole pattern, indicating a shift in position.



The diabatic intensification of the blocks in CNTRL goes along with an amplified upper-level anticyclonic circulation. The differences in the rotational wind around the negative PV differences inside the block clearly reveal the intensified anticyclonic flow associated with the intense negative PV anomalies of the CTNRL simulations, especially on the flanks with substantial wind speed differences of up to 40 m s^{-1} between CTNRL and NOLH (see wind vectors in Fig. 8).

355 In the following, we have a closer look at the individual cases. In Thor onset (Fig. 8a), negative PV differences inside the block and positive differences south of it indicate the anticyclonic wrap-up of low- over high-PV air and the formation of a dipole block with easterly winds in CNTRL, while in NOLH the negative PV anomaly is detached further north above Svalbard as a tropospheric cut-off. In Thor maintenance (Fig. 8b), the block is still present in CNTRL while it is already too weak to be detected in NOLH. The poleward elongation of the CNTRL block is reflected in the negative PV difference (ΔPV up to
360 -4 pvu) with an anticyclonic flow centered over Iceland. In NOLH, the decaying blocking ridge over Europe and the cut-off PV anomaly east of Greenland do not merge. For the case Canada (Fig. 8c), the omega-shaped structure of the block with tilted upstream and downstream troughs is not reproduced without LH, and the NOLH block develops as an open ridge embedded in a Rossby wave with a weak anticyclonic circulation over western Canada. In the case of Russia (Fig. 8e), the initial PV differences over western Europe have propagated eastward and reach values of -5 pvu over western Russia at day 6, with a
365 strong anticyclonic flow only present when LH is included. In contrast to the other cases, the PV values inside the block's core are similar in CNTRL and NOLH for the Cold spell case (Fig. 8d). Largest negative PV differences are found along the edge of the block, i.e. the block is smaller in spatial extent in NOLH, and further south over the Azores, where the NOLH block detaches from the tropospheric reservoir.

Interestingly, a common feature in several NOLH simulations (Thor onset, Thor maintenance, Cold spell and Russia) is the
370 formation of a low-PV anomaly in the northern part of the domain that is cut off from its tropospheric source and surrounded by high-PV stratospheric air (Fig. 8a,b,d,e). These cut-off anomalies are formed when the jet stream is retreating back to a more zonal flow. In contrast to the CNTRL simulations, they are not accompanied by a cyclonic anomaly to the south, and therefore do not constitute a stationary dipolar flow pattern that generates stronger easterlies at the primary latitude of the jet. The typical inverse-S shape of the 2 pvu contour during overturning Rossby waves, which is used to describe blocking in association with
375 wave breaking (e.g., Pelly and Hoskins, 2003) is only simulated with the inclusion of LH. This again highlights the role of LH in effectively displacing the jet stream far to the north and promoting persistent Rossby wave breaking.

4.2.2 Differences in PV advection by the divergent outflow

For a quantitative analysis of the effect of LH on vertical motion and upper-level PV advection by the divergent outflow, upper-level vertical wind (ω), upper-level divergent wind (\mathbf{v}_χ) and associated PV advection by the divergent wind ($\mathbf{v}_\chi \cdot \nabla PV$) are
380 determined in a region on the western flank of the blocking ridge for all cases. The respective values are averaged over a $3^\circ \times 3^\circ$ box centered around the strongest ascent, largest divergent wind, and strongest negative PV advection found on the western flank of the individual tracked blocks, respectively. Figure 9 shows their temporal evolution for the CNTRL (solid lines) and NOLH (dashed lines) simulations. Without LH, almost all NOLH curves flatten out. Vertical wind ω (Fig. 9a) is reduced locally by up to 75 %, accompanied by a strong reduction in divergent outflow aloft (Fig. 9b). Consequently, the negative PV



385 advection is almost absent in NOLH (Fig. 9c). The exception is the Russia block (magenta curves), where the removal of LH hardly changes the strength of ω and \mathbf{v}_χ after the onset (day 3). As the block propagates downstream over Russia and away from the storm track region over the ocean basin, the influence of direct diabatic injection of low-PV air in WCBs is reduced, and quasi-adiabatic dynamics, i.e., cooling along upper-level air masses (see Fig. 10b in next subsection) dominate in both CNTRL and NOLH.

390 4.2.3 Differences in blocking characteristics

Figure 10 shows a quantitative comparison of the temporal evolution of blocking characteristics (LH contribution, mean diabatic heating, intensity and spatial extent) obtained from the CNTRL (solid lines) and NOLH (dashed lines). Note that the individual curves start as soon as a block is identified with the APV index (see section 2) in the corresponding simulation. Characteristics based on 3-day backward trajectories (LH contribution and diabatic heating) can only be obtained after at least
395 3 days of model integration time.

The episodic nature of LH contribution and diabatic heating (Fig. 10a,b) during the blocking life cycle in the different CNTRL simulations is associated with the passage of synoptic cyclones and the associated cross-isentropic transport of low-PV air in WCBs. LH bursts (local maxima of LH contribution and diabatic heating) typically indicate the time of strongest interaction between the block and the approaching upstream cyclones (see also Steinfeld and Pfahl, 2019). The periods between such LH
400 bursts are dominated by a median cooling of -3 to -4 K and predominantly quasi-horizontal transport of near-tropopause air masses (see again trajectories in Fig. 5). The relative importance of LH varies strongly during the lifetime of the blocks and from system to system. Consistent with previous observational work (e.g., Colucci, 1985; Lupu and Smith, 1995), all blocking cases are initiated by upstream cyclogenesis. As discussed above, Thor onset is associated with two upstream cyclones, one during onset (day 3) and one during the second intensification phase (day 6), and Thor maintenance interacts with 3 upstream
405 eddies at days 1 (for which no backward trajectories can be calculated), 4 and 6. For the Cold spell case, two North Atlantic upstream cyclones are present during onset (day 3) and the second intensification phase (day 6). The Canada case is only affected by one North Pacific upstream cyclone during onset (day 3), but this cyclone moves slowly and influences the block for the next 4 days. The block in the Russia case is initiated by a North Atlantic cyclone during day 3 - 4, it then propagates eastward and further interacts with a second upstream cyclone during day 6, however diabatic cooling dominates.

410 Considering all the blocks in the CNTRL simulations, 43 % of their air masses experience heating of more than 2 K in 3 days with a median heating of 11 K and with a wide range of $\Delta\theta$ up to 45 K. In the NOLH simulations, the LH contribution is reduced to 15 % with a median heating of 3 K (dashed curves in Fig. 10a,b). The other 85 % of the air masses experience diabatic cooling of ~ 4 K in the median (Fig. 10b).

Comparing the evolution of block intensity and spatial extent between CNTRL and NOLH shows that LH leads to more
415 intense and larger blocks with an extended lifetime (Fig. 10c,d). In the CNTRL simulations, blocking ridges intensify more rapidly and PV anomalies are thus stronger and spatially more extended compared to their counterparts without LH. Generally, the differences in intensity and spatial extent between NOLH and CNTRL increase with model integration time, resulting in a 10 (Cold spell) to 40 % (Canada) reduction in intensity and a 30 (Cold spell) to 80 % (Thor onset and maintenance) reduction



in spatial extent during the mature phase. However, the experiments indicate a large case-to-case variability with respect to the
420 sensitivity of the block to LH. Without LH, the Thor and Cold spell blocks develop later with a delay of about 1 and 4 days,
respectively, because the first ridge amplification is too weak and only later, when a second upstream cyclone is approaching,
the anomaly becomes strong enough. The Thor maintenance block experiences a quick reduction in amplitude without LH, and
dissipates 4 days earlier than the CNTRL block. The Canada block has its onset at the same time in both CNTRL and NOLH
425 simulations, however the ridge does not further amplify in NOLH. Likewise, the Russia block has a delayed onset and does
not strongly amplify without LH. For the Cold spell block, once the blocking develops in NOLH (around day 6) differences
in intensity and spatial extent compared to CNTRL do not grow substantially with lead time. This case is special, as a block
with similar intensity develops in both CNTRL and NOLH simulations (see again Fig. 8d). As mentioned above, in all cases,
except for Cold spell, the tracked negative PV anomalies are not classified as blocking in the NOLH simulations when using
430 the original blocking index of Schwierz et al. (2004a), because the PV anomalies are too weak, do not persist for more than 5
days, and/or are too mobile.

Since the characteristics of the block can develop differently, it is difficult to quantify which event is most sensitive to
changes in LH. The effect of LH on blocking intensity and extent appears to depend on the phase of the blocking life cycle,
on the intensity of the upstream cyclone, and the state of the background flow. During the early growth phase with an initially
zonal and intense upper-level jet stream, cloud diabatic heating intensifies the upstream cyclone and facilitates a faster growth
435 of the ridges. However, during the mature phase when the large-scale flow is already in an amplified state, Thor onset and Cold
spell blocks amplify without the contribution of LH, and thus they appear less sensitive to changes in LH. The presence of an
amplified ridge with a large-scale upper-level diffluent flow is known to provide a favorable environment for blocking initiation
and maintenance (Colucci, 1985; Pelly and Hoskins, 2003), which supports the meridional amplification of the upstream waves
[eddy straining mechanism, Shutts (1983)] and the poleward transport of air with low PV (Yamazaki and Itoh, 2012; Steinfeld
440 and Pfahl, 2019), and the block can thus also form in the absence of intense LH. However, in the Thor onset case there is still
a big difference in the large-scale flow evolution between the simulations (dipole block in CNTRL vs cut-off low-PV anomaly
in NOLH), despite similar blocking intensities around day 6. Despite the strong case-to-case variability in the LH contribution
and in the sensitivity of the blocks to changes in LH, the experiments demonstrate that LH can have a profound causal effect
on blocking intensity, spatial extent and lifetime.

445 5 Conclusions

The relative roles of different processes for the formation and maintenance of atmospheric blocking have been debated for a
long time (Woollings et al., 2018). While classical blocking theories are based on dry-adiabatic interactions of waves (e.g.,
Charney and DeVore, 1979; Shutts, 1983), the importance of moist-diabatic processes, in particular the release of latent heat
in ascending airstreams, has recently been recognized to play a significant role in the dynamics of the upper-level large-scale
450 flow, including Rossby waves (e.g., Pomroy and Thorpe, 2000; Grams et al., 2011; Wirth et al., 2018) and blocking (Pfahl
et al., 2015; Quinting and Reeder, 2017; Steinfeld and Pfahl, 2019; Müller and Névir, 2019). Motivated by this recent finding,



the present study explores the causal effect of latent heating on the development of five different blocking cases with the help of sensitivity experiments with a global numerical model.

A key finding of the numerical sensitivity experiments is that the intensity, spatial extent and lifetime of all simulated
455 blocking events depends strongly on latent heating. In some cases (in 4 of 5 cases), the presence of LH even determines whether or not blocking (according to the blocking index of Schierz et al. (2004a)) occurs at all. Consistent with the findings of previous studies (Davis et al., 1993; Stoelinga, 1996; Pauley and Smith, 1988; Pomroy and Thorpe, 2000), the primary effects of latent heating on the tropopause arise from the diabatic reduction of PV and the associated enhancement of the divergent outflow aloft. Latent heating enhances the vertical motion and divergent outflow on the western flank of the block, locally by
460 a factor 4, and the succeeding interaction with the upper-level PV distribution modifies the amplification and propagation of blocking compared to the simulations without latent heating. These processes act to slow down the eastward propagation and amplify the intensity and extent of the negative PV anomaly in all cases.

A comparison between the five cases reveals a large case-to-case variability of the effect of latent heating on blocking, which depends strongly on the phase of the blocking life cycle and the state of the background flow. During the early growth phase,
465 latent heating contributes to the initial ridge amplification and facilitates a faster growth of the incipient ridge. During the mature phase, on the other hand, the large-scale flow can further amplify also without the contribution of LH and thus appears to be less sensitive to changes in LH. This amplification is related to the state of the background flow: In the cases with a more meridional flow and a pre-existing large-scale ridge, a block also develops in the absence of latent heating, though weaker and less extended. The presence of this pre-existing ridge induces large-scale upper-level deformation (diffluent flow), which
470 supports the meridional amplification of arriving synoptic-scale waves (eddy straining mechanism Shutts, 1983; Mullen, 1987) and the poleward quasi-adiabatic transport of low-PV air from lower latitudes ahead of baroclinic disturbances (e.g., Colucci, 1985). Nevertheless, as demonstrated in the case study of the maintenance of block Thor, the absence of latent heating can also lead to a more rapid decay of blocking. In this case, the dry-adiabatic forcing due to eddy straining in the diffluent region upstream of the block is not strong enough to sustain the system against dissipation.

475 These different case studies demonstrate that blocking is the result of a constructive interaction between diabatic heating and dry baroclinic processes. Intense latent heating occurs predominantly in the warm conveyor belt of extratropical cyclones (Wernli, 1997) and is thus in phase with and strongly coupled to the secondary circulation associated with dry adiabatic forcing (Kuo et al., 1990). Our sensitivity experiments corroborate earlier studies that the interaction between mobile synoptic-scale eddies and planetary-scale flow anomalies plays an important role for blocking formation and maintenance (Nakamura et al.,
480 1997; Luo et al., 2014; Nakamura and Huang, 2018), and show that diabatic processes can provide the required flow amplification in addition to dry-dynamical forcing. In order to properly represent blocking dynamics, numerical weather prediction and climate models thus have to correctly account for this coupling between dry and moist processes, including the details of microphysical processes that shape the spatial distribution of latent heating in clouds (e.g., Joos and Wernli, 2012; Dearden et al., 2016; Joos and Forbes, 2016; Crezee et al., 2017; Attinger et al., 2019).



485 *Code and data availability.* The blocking identification code CONTRACK is available from <https://svn.iac.ethz.ch/websvn/pub>. The code and information on how to use the Lagrangian Analysis tool LAGRANTO can be found from <http://www.lagranto.ethz.ch>. The data of the IFS sensitivity simulations is available from Daniel Steinfeld upon request.

Author contributions. D. Steinfeld performed the numerical experiments, analysed the data and wrote the paper. M. Boettcher, R. Forbes and S. Pfahl provided guidance on interpreting the result. All authors commented on the manuscript.

490 *Competing interests.* The authors declare no conflict of interest.

Acknowledgements. D. Steinfeld acknowledges funding from ETH Research Grant ETH-09 15-2. We thank Elisa Spreitzer, Roman Attinger, Hanna Joos and Heini Wernli (ETH Zürich) and Christian Grams (KIT) for fruitful discussions on diabatic processes in mid-latitude weather systems. IFS model simulations have been performed as part of the ECMWF special project "Diabatic effects in mid-latitude weather systems". ECMWF and MeteoSwiss are acknowledged for making the IFS model available and for access to the ECMWF computing facilities. The data analysis and visualization was done using Python.

495



References

- Ahlgrimm, M. and Forbes, R.: Improving the Representation of Low Clouds and Drizzle in the ECMWF Model Based on ARM Observations from the Azores, *Mon. Weather Rev.*, 142, 668–685, <https://doi.org/10.1175/MWR-D-13-00153.1>, 2013.
- Ahmadi-Givi, F., Graig, G. C., and Plant, R. S.: The dynamics of a midlatitude cyclone with very strong latent-heat release, *Q. J. R. Meteorol. Soc.*, 130, 295–323, <https://doi.org/10.1256/qj.02.226>, 2004.
- Altenhoff, A. M., Martius, O., Croci-Maspoli, M., Schwierz, C., and Davies, H. C.: Linkage of atmospheric blocks and synoptic-scale Rossby waves: a climatological analysis, *Tellus A*, 60, 1053–1063, <https://doi.org/10.1111/j.1600-0870.2008.00354.x>, 2008.
- Archambault, H. M., Bosart, L. F., Keyser, D., and Cordeira, J. M.: A climatological analysis of the extratropical flow response to recurving western north pacific tropical cyclones, *Mon. Weather Rev.*, 141, 2325–2346, <https://doi.org/10.1175/MWR-D-12-00257.1>, 2013.
- Attinger, R., Spreitzer, E., Boettcher, M., Forbes, R., Wernli, H., and Joos, H.: Quantifying the role of individual diabatic processes for the formation of PV anomalies in a North Pacific cyclone, *Q. J. R. Meteorol. Soc.*, 145, 0035–9009, <https://doi.org/doi:10.1002/qj.3573>, 2019.
- Bechtold, P., Köhler, M., Jung, T., Doblas-Reyes, F., Leutbecher, M., Rodwell, M. J., Vitart, F., and Balsamo, G.: Advances in simulating atmospheric variability with the ECMWF model: From synoptic to decadal time-scales, *Q. J. R. Meteorol. Soc.*, 134, 1337–1351, <https://doi.org/10.1002/qj.289>, 2008.
- Bechtold, P., Semane, N., Lopez, P., Chaboureau, J.-P., Beljaars, A., and Bormann, N.: Representing equilibrium and nonequilibrium convection in large-scale Models, *J. Atmos. Sci.*, 71, 734–753, <https://doi.org/10.1175/JAS-D-13-0163.1>, 2013.
- Berggren, R., Bolin, B., and Rossby, C.-G.: An aerological study of zonal motion, its perturbations and break-down, *Tellus*, 1, 14–37, <https://doi.org/10.1111/j.2153-3490.1949.tb01257.x>, 1949.
- Binder, H., Boettcher, M., Joos, H., and Wernli, H.: The role of warm conveyor belts for the intensification of extratropical cyclones in Northern Hemisphere winter, *J. Atmos. Sci.*, 73, 3997–4020, <https://doi.org/10.1175/JAS-D-15-0302.1>, 2016.
- Büeler, D. and Pfahl, S.: Potential vorticity diagnostics to quantify effects of latent heating in extratropical cyclones. Part I: methodology, *J. Atmos. Sci.*, 74, 3567–3590, <https://doi.org/10.1175/JAS-D-17-0041.1>, 2017.
- Charney, J. G. and DeVore, J. G.: Multiple flow equilibria in the atmosphere and blocking, *J. Atmos. Sci.*, 36, 1205–1216, [https://doi.org/10.1175/1520-0469\(1979\)036<1205:MFEITA>2.0.CO;2](https://doi.org/10.1175/1520-0469(1979)036<1205:MFEITA>2.0.CO;2), 1979.
- Colucci, S. J.: Explosive cyclogenesis and large-scale circulation changes: implications for atmospheric blocking, *J. Atmos. Sci.*, 42, 2701–2717, [https://doi.org/10.1175/1520-0469\(1985\)042<2701:ECALSC>2.0.CO;2](https://doi.org/10.1175/1520-0469(1985)042<2701:ECALSC>2.0.CO;2), 1985.
- Crezee, B., Joos, H., and Wernli, H.: The Microphysical Building Blocks of Low-Level Potential Vorticity Anomalies in an Idealized Extratropical Cyclone, *J. Atmos. Sci.*, 74, 1403–1416, <https://doi.org/10.1175/JAS-D-16-0260.1>, 2017.
- Croci-Maspoli, M., Schwierz, C., and Davies, H. C.: A multifaceted climatology of atmospheric blocking and its recent linear trend, *J. Clim.*, 20, 633–649, <https://doi.org/10.1175/JCLI4029.1>, 2007.
- Davis, C. A., Stoelinga, M. T., and Kuo, Y.-H.: The integrated effect of condensation in numerical simulations of extratropical cyclogenesis, *Mon. Weather Rev.*, 121, 2309–2330, [https://doi.org/10.1175/1520-0493\(1993\)121<2309:TIEOCI>2.0.CO;2](https://doi.org/10.1175/1520-0493(1993)121<2309:TIEOCI>2.0.CO;2), 1993.
- Dearden, C., Vaughan, G., Tsai, T., and Chen, J.-P.: Exploring the diabatic role of ice microphysical processes in two North Atlantic summer cyclones, *Mon. Weather Rev.*, 144, 1249–1272, <https://doi.org/10.1175/MWR-D-15-0253.1>, 2016.
- Dee, D. P., Uppala, S. M., Simmons, A. J., Berrisford, P., Poli, P., Kobayashi, S., Andrae, U., Balmaseda, M. A., Balsamo, G., Bauer, P., Bechtold, P., Beljaars, A. C. M., van de Berg, L., Bidlot, J., Bormann, N., Delsol, C., Dragani, R., Fuentes, M., Geer, A. J., Haimberger, L., Healy, S. B., Hersbach, H., Hólm, E. V., Isaksen, L., Kållberg, P., Köhler, M., Matricardi, M., McNally, A. P., Monge-Sanz, B. M., Mor-



- crette, J. J., Park, B. K., Peubey, C., de Rosnay, P., Tavalato, C., Thépaut, J. N., and Vitart, F.: The ERA-Interim reanalysis: configuration and performance of the data assimilation system, *Q. J. R. Meteorol. Soc.*, 137, 553–597, <https://doi.org/10.1002/qj.828>, 2011.
- 535 Dole, R. M.: The life cycles of persistent anomalies and blocking over the North Pacific, *Adv. Geophys.*, 29, 31–69, [https://doi.org/10.1016/S0065-2687\(08\)60034-5](https://doi.org/10.1016/S0065-2687(08)60034-5), 1986.
- Drouard, M. and Woollings, T.: Contrasting mechanisms of summer blocking over western Eurasia, *Geophys. Res. Lett.*, 45, 12,12–40,48, <https://doi.org/10.1029/2018GL079894>, 2018.
- ECMWF: IFS documentation CY43r1, available at: <https://www.ecmwf.int/en/elibrary/17117-part-iv-physical-processes>, 2016.
- 540 EUMETSAT: Cloud top height product: Product guide, 2017.
- Forbes, R. M. and Ahlgrim, M.: On the representation of high-latitude boundary layer mixed-phase cloud in the ECMWF global model, *Mon. Weather Rev.*, 142, 3425–3445, <https://doi.org/10.1175/MWR-D-13-00325.1>, 2014.
- Forbes, R. M., Tompkins, A. M., and Untch, A.: A new prognostic bulk microphysics scheme for the IFS., Tech. rep., ECMWF, 2011.
- Grams, C. M., Wernli, H., Böttcher, M., Čampa, J., Corsmeier, U., Jones, S. C., Keller, J. H., Lenz, C.-J., and Wiegand, L.: The key role of
545 diabatic processes in modifying the upper-tropospheric wave guide: a North Atlantic case-study, *Q. J. R. Meteorol. Soc.*, 137, 2174–2193, <https://doi.org/10.1002/qj.891>, 2011.
- Green, J. S. A.: The weather during July 1976: Some dynamical consideration of the drought, *Weather*, 32, 120–126, <https://doi.org/10.1002/j.1477-8696.1977.tb04532.x>, 1977.
- Hoskins, B. J. and Valdes, P. J.: On the existence of storm-tracks, *J. Atmos. Sci.*, 47, 1854–1864, [https://doi.org/10.1175/1520-0469\(1990\)047<1854:OTEOST>2.0.CO;2](https://doi.org/10.1175/1520-0469(1990)047<1854:OTEOST>2.0.CO;2), 1989.
- 550 Hoskins, B. J., James, I. N., and White, G. H.: The shape, propagation and mean-flow interaction of large-scale weather systems, *J. Atmos. Sci.*, 40, 1595–1612, [https://doi.org/10.1175/1520-0469\(1983\)040<1595:TSPAMF>2.0.CO;2](https://doi.org/10.1175/1520-0469(1983)040<1595:TSPAMF>2.0.CO;2), 1983.
- Hoskins, B. J., McIntyre, M. E., and Robertson, A. W.: On the use and significance of isentropic potential vorticity maps, *Q. J. R. Meteorol. Soc.*, 111, 877–946, <https://doi.org/10.1002/qj.49711146602>, 1985.
- 555 Joos, H. and Forbes, R. M.: Impact of different IFS microphysics on a warm conveyor belt and the downstream flow evolution, *Q. J. R. Meteorol. Soc.*, 142, 2727–2739, <https://doi.org/10.1002/qj.2863>, 2016.
- Joos, H. and Wernli, H.: Influence of microphysical processes on the potential vorticity development in a warm conveyor belt: A case-study with the limited-area model COSMO, *Q. J. R. Meteorol. Soc.*, 138, 407–418, <https://doi.org/10.1002/qj.934>, 2012.
- Kuo, Y.-H., Shapiro, M. A., and Donall, E. G.: The interaction between baroclinic and diabatic processes in a numerical sim-
560 ulation of a rapidly intensifying extratropical marine cyclone, *Mon. Weather Rev.*, 119, 368–384, [https://doi.org/10.1175/1520-0493\(1991\)119<0368:TIBBAD>2.0.CO;2](https://doi.org/10.1175/1520-0493(1991)119<0368:TIBBAD>2.0.CO;2), 1990.
- Luo, D., Cha, J., Zhong, L., and Dai, A.: A nonlinear multiscale interaction model for atmospheric blocking: The eddy-blocking matching mechanism, *Q. J. R. Meteorol. Soc.*, 140, 1785–1808, <https://doi.org/10.1002/qj.2337>, 2014.
- Lupo, A. R. and Smith, P. J.: Climatological features of blocking anticyclones in the Northern Hemisphere, *Tellus A*, 47, 439–456,
565 <https://doi.org/10.1034/j.1600-0870.1995.t01-3-00004.x>, 1995.
- Maddison, J. W., Gray, S. L., Martínez-Alvarado, O., and Williams, K. D.: Upstream cyclone influence on the predictability of block onsets over the Euro-Atlantic region, *Mon. Weather Rev.*, 147, 1277–1296, <https://doi.org/10.1175/MWR-D-18-0226.1>, 2019.
- Madonna, E., Wernli, H., Joos, H., and Martius, O.: Warm conveyor belts in the ERA-Interim Dataset (1979–2010). Part I: Climatology and potential vorticity evolution, *J. Clim.*, 27, 3–26, <https://doi.org/10.1175/JCLI-D-12-00720.1>, 2014.



- 570 Martius, O., Schwierz, C., and Davies, H. C.: Tropopause-level waveguides, *J. Atmos. Sci.*, 67, 866–879, <https://doi.org/10.1175/2009JAS2995.1>, 2010.
- Mullen, S.: Transient eddy forcing of blocking flows, *J. Atmos. Sci.*, 44, 3–22, [https://doi.org/10.1175/1520-0469\(1987\)044<0003:TEFOBF>2.0.CO;2](https://doi.org/10.1175/1520-0469(1987)044<0003:TEFOBF>2.0.CO;2), 1987.
- Müller, A. and Névir, P.: Using the concept of the Dynamic State Index for a scale-dependent analysis of atmospheric blocking, *Meteorol. Zeitschrift*, 28, 487–498, <https://doi.org/10.1127/metz/2019/0963>, 2019.
- 575 Nakamura, H. and Wallace, J. M.: Synoptic behavior of baroclinic eddies during the blocking onset, *Mon. Weather Rev.*, 121, 1892–1903, [https://doi.org/10.1175/1520-0493\(1993\)121<1892:SBOBED>2.0.CO;2](https://doi.org/10.1175/1520-0493(1993)121<1892:SBOBED>2.0.CO;2), 1993.
- Nakamura, H., Nakamura, M., and Anderson, J. L.: The role of high- and low-frequency dynamics in blocking formation, *Mon. Weather Rev.*, 125, 2074–2093, [https://doi.org/10.1175/1520-0493\(1997\)125<2074:TROHAL>2.0.CO;2](https://doi.org/10.1175/1520-0493(1997)125<2074:TROHAL>2.0.CO;2), 1997.
- 580 Nakamura, N. and Huang, C. S.: Atmospheric blocking as a traffic jam in the jet stream, *Science*, 361, 42–47, <https://doi.org/10.1126/science.aat0721>, 2018.
- Pauley, P. M. and Smith, P. J.: Direct and indirect effects of latent heat release on a synoptic-scale wave system, *Mon. Weather Rev.*, 116, 1209–1236, [https://doi.org/10.1175/1520-0493\(1988\)116<1209:DAIEOL>2.0.CO;2](https://doi.org/10.1175/1520-0493(1988)116<1209:DAIEOL>2.0.CO;2), 1988.
- Pelly, J. L. and Hoskins, B. J.: A new perspective on blocking, *J. Atmos. Sci.*, 60, 743–755, [https://doi.org/10.1175/1520-0469\(2003\)060<0743:ANPOB>2.0.CO;2](https://doi.org/10.1175/1520-0469(2003)060<0743:ANPOB>2.0.CO;2), 2003.
- 585 Petoukhov, V., Rahmstorf, S., Petri, S., and Schellnhuber, H. J.: Quasiresonant amplification of planetary waves and recent Northern Hemisphere weather extremes, *Proc. Natl. Acad. Sci.*, 110, 5336–5341, <https://doi.org/10.1073/pnas.1222000110>, 2013.
- Pfahl, S., Schwierz, C., Croci-Maspoli, M., Grams, C. M., and Wernli, H.: Importance of latent heat release in ascending air streams for atmospheric blocking, *Nat. Geosci.*, 8, 610–614, <https://doi.org/10.1038/ngeo2487>, 2015.
- 590 Pomroy, H. R. and Thorpe, A. J.: The evolution and dynamical role of reduced upper-tropospheric potential vorticity in intensive observing period one of FASTEX, *Mon. Weather Rev.*, 128, 1817–1834, [https://doi.org/10.1175/1520-0493\(2000\)128<1817:TEADRO>2.0.CO;2](https://doi.org/10.1175/1520-0493(2000)128<1817:TEADRO>2.0.CO;2), 2000.
- Quinting, J. F. and Reeder, M. J.: Southeastern Australian heat waves from a trajectory viewpoint, *Mon. Weather Rev.*, 145, 4109–4125, <https://doi.org/10.1175/MWR-D-17-0165.1>, 2017.
- 595 Rex, D. F.: Blocking action in the middle troposphere and its effect upon regional climate, *Tellus*, 2, 196–211, <https://doi.org/10.1111/j.2153-3490.1950.tb00331.x>, 1950.
- Riemer, M., Jones, S. C., and Davis, C. A.: The impact of extratropical transition on the downstream flow: An idealized modelling study with a straight jet, *Q. J. R. Meteorol. Soc.*, 134, 69–91, <https://doi.org/10.1002/qj.189>, 2008.
- Rodwell, M. J., Magnusson, L., Bauer, P., Bechtold, P., Bonavita, M., Cardinali, C., Diamantakis, M., Earnshaw, P., Garcia-Mendez, A.,
- 600 Isaksen, I., Källén, E., Klocke, D., Lopez, P., McNally, T., Persson, A., Prates, F., and Wedi, N.: Characteristics of occasional poor medium-range weather forecasts for Europe, *Bull. Am. Meteorol. Soc.*, 94, 1393–1405, <https://doi.org/10.1175/BAMS-D-12-00099.1>, 2013.
- Schäfer, A., Craig, G., Wernli, H., Arbogast, P., Doyle, J. D., McTaggart-Cowan, R., Methven, J., Rivière, G., Ament, F., Boettcher, M., Bramberger, M., Cazenave, Q., Cotton, R., Crewell, S., Delanoë, J., Dörnbrack, A., Ehrlich, A., Ewald, F., Fix, A., Grams, C. M., Gray,
- 605 S. L., Grob, H., Groß, S., Hagen, M., Harvey, B., Hirsch, L., Jacob, M., Kölling, T., Konow, H., Lemmerz, C., Lux, O., Magnusson, L., Mayer, B., Mech, M., Moore, R., Pelon, J., Quinting, J., Rahm, S., Rapp, M., Rautenhaus, M., Reitebuch, O., Reynolds, C. A., Sodemann,



- H., Spengler, T., Vaughan, G., Wendisch, M., Wirth, M., Witschas, B., Wolf, K., and Zinner, T.: The North Atlantic Waveguide and Downstream Impact Experiment, *Bull. Am. Meteorol. Soc.*, 99, 1607–1637, <https://doi.org/10.1175/BAMS-D-17-0003.1>, 2018.
- 610 Scherrer, S. C., Croci-Maspoli, M., Schwierz, C., and Appenzeller, C.: Two-dimensional indices of atmospheric blocking and their statistical relationship with winter climate patterns in the Euro-Atlantic region, *Int. J. Climatol.*, 26, 233–249, <https://doi.org/10.1002/joc.1250>, 2006.
- Schwierz, C., Croci-Maspoli, M., and Davies, H. C.: Perspicacious indicators of atmospheric blocking, *Geophys. Res. Lett.*, 31, 0094–8276, <https://doi.org/10.1029/2003GL019341>, 2004a.
- Schwierz, C., Dirren, S., and Davies, H. C.: Forced Waves on a Zonally Aligned Jet Stream, *J. Atmos. Sci.*, 61, 73–87, 615 [https://doi.org/10.1175/1520-0469\(2004\)061<0073:FWOAZA>2.0.CO;2](https://doi.org/10.1175/1520-0469(2004)061<0073:FWOAZA>2.0.CO;2), 2004b.
- Shutts, G. J.: The propagation of eddies in diffuent jetstreams : eddy vorticity forcing of blocking flow fields, *Q. J. R. Meteorol. Soc.*, 109, 737–761, <https://doi.org/10.1002/qj.49710946204>, 1983.
- Spreitzer, E., Attinger, R., Boettcher, M., Forbes, R., Wernli, H., and Joos, H.: Modification of potential vorticity near the tropopause by non-conservative processes in the ECMWF model, *J. Atmos. Sci.*, 76, 1709–1726, 2019.
- 620 Sprenger, M. and Wernli, H.: The LAGRANTO Lagrangian analysis tool – version 2.0, *Geosci. Model Dev.*, 8, 2569–2586, <https://doi.org/10.5194/gmd-8-2569-2015>, 2015.
- Steinfeld, D. and Pfahl, S.: The role of latent heating in atmospheric blocking dynamics: a global climatology, *Clim. Dyn.*, 53, 6159–6180, <https://doi.org/10.1007/s00382-019-04919-6>, 2019.
- Stoelinga, M. T.: A Potential Vorticity-Based Study of the Role of Diabatic Heating and Friction in a Numerically Simulated Baroclinic Cyclone, *Mon. Weather Rev.*, 124, 849–874, [https://doi.org/10.1175/1520-0493\(1996\)124<0849:APVBSO>2.0.CO;2](https://doi.org/10.1175/1520-0493(1996)124<0849:APVBSO>2.0.CO;2), 1996.
- 625 Teubler, F. and Riemer, M.: Dynamics of Rossby wave packets in a quantitative potential vorticity-potential temperature framework, *J. Atmos. Sci.*, 73, 1063–1081, <https://doi.org/10.1175/JAS-D-15-0162.1>, 2016.
- Tiedtke, M.: A comprehensive mass flux scheme for cumulus parameterization in large-scale models, *Mon. Weather Rev.*, 117, 1779–1800, [https://doi.org/10.1175/1520-0493\(1989\)117<1779:ACMFSF>2.0.CO;2](https://doi.org/10.1175/1520-0493(1989)117<1779:ACMFSF>2.0.CO;2), 1989.
- 630 Tiedtke, M.: Representation of clouds in large-scale models, *Mon. Weather Rev.*, 121, 3040–3061, [https://doi.org/10.1175/1520-0493\(1993\)121<3040:ROCILS>2.0.CO;2](https://doi.org/10.1175/1520-0493(1993)121<3040:ROCILS>2.0.CO;2), 1993.
- Tyrlis, E. and Hoskins, B. J.: The morphology of Northern Hemisphere blocking, *J. Atmos. Sci.*, 65, 1653–1665, <https://doi.org/10.1175/2007JAS2338.1>, 2008.
- Wernli, H.: A Lagrangian-based analysis of extratropical cyclones. II: a detailed case-study, *Q. J. R. Meteorol. Soc.*, 123, 1677–1706, 635 <https://doi.org/10.1002/qj.49712354211>, 1997.
- Wernli, H. and Davies, H. C.: A Lagrangian-based analysis of extratropical cyclones. I: the method and some applications, *Q. J. R. Meteorol. Soc.*, 123, 467–489, 1997.
- Wirth, V., Riemer, M., Chang, E. K. M., and Martius, O.: Rossby wave packets on the midlatitude waveguide—a review, *Mon. Weather Rev.*, 146, 1965–2001, <https://doi.org/10.1175/MWR-D-16-0483.1>, 2018.
- 640 Woollings, T., Barriopedro, D., Methven, J., Son, S.-W., Martius, O., Harvey, B., Sillmann, J., Lupo, A. R., and Seneviratne, S.: Blocking and its response to climate change, *Curr. Clim. Chang. Reports*, 4, 287–300, <https://doi.org/10.1007/s40641-018-0108-z>, 2018.
- Yamazaki, A. and Itoh, H.: Vortex - Vortex interactions for the maintenance of blocking. Part I: the selective absorption mechanism and a case study, *J. Atmos. Sci.*, 70, 725–742, <https://doi.org/10.1175/JAS-D-11-0295.1>, 2012.

<https://doi.org/10.5194/wcd-2020-5>
Preprint. Discussion started: 17 February 2020
© Author(s) 2020. CC BY 4.0 License.



Zhang, G. and Wang, Z.: North Atlantic extratropical Rossby wave breaking during the warm season: wave life cycle and role of diabatic heating, *Mon. Weather Rev.*, 146, 695–712, <https://doi.org/10.1175/MWR-D-17-0204.1>, 2018.

645

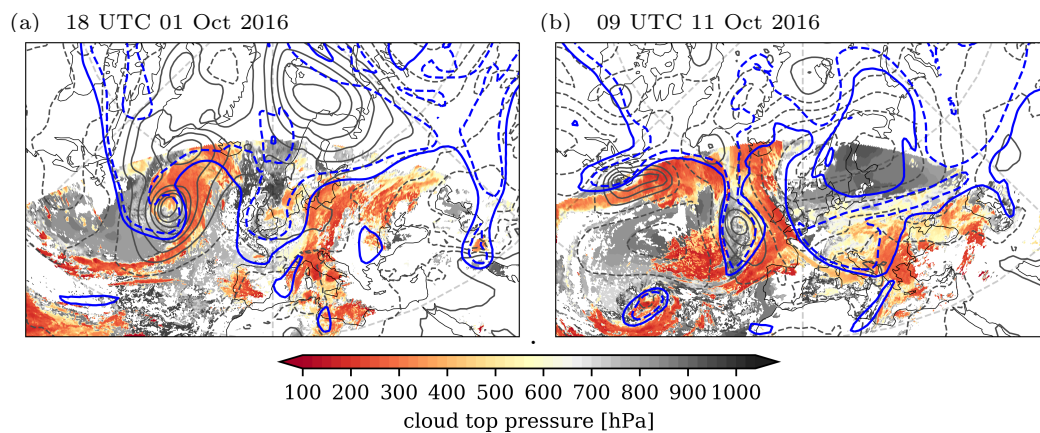


Figure 1. Synoptic situation over the North Atlantic at a) 18 UTC 01 Oct 2016 and b) 9 UTC 11 Oct 2016. SLP (gray contours, every 10 hPa, solid to dashed contours at 1015 hPa) and upper-level PV (blue contours, 2 (solid) and 3 (dashed) pvu) from the IFS CNTRL run. Cloud top heights (hPa, shading) from satellite imagery based on EUMETSAT MSG-SEVIRI data (EUMETSAT, 2017).

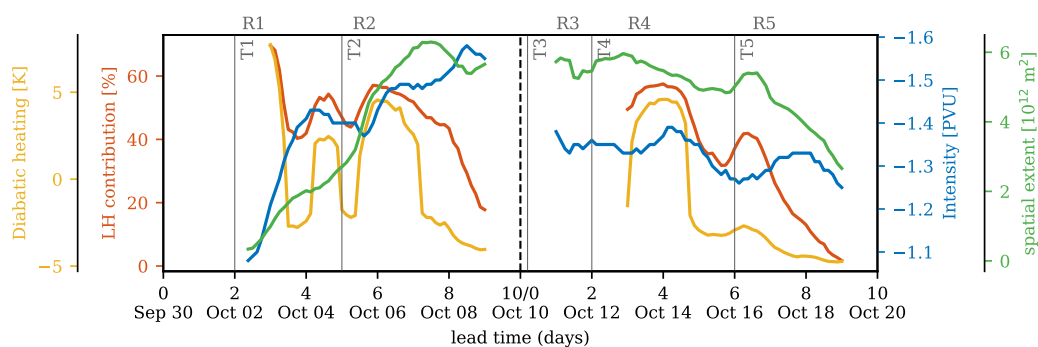


Figure 2. Percentage of trajectories with $\Delta\theta > 2$ K in 3 days (red, %), mean diabatic heating along the blocking trajectories (yellow, K), blocking intensity (blue, right axis, pvu), and spatial extent (green, 2nd right axis, 10^{12}m^2) as a function of time (simulation lead time and date) for Thor onset and maintenance. Note that 3-day backward trajectories can only be calculated after day 3. Labels “T1 - T5” and “R1 - R5” refer to the cyclones and ridges during time of their interaction with block Thor. Note that no block is detected between 9–11 October as a result of the 2-day temporal smoothing of the upper-level PV anomaly field.

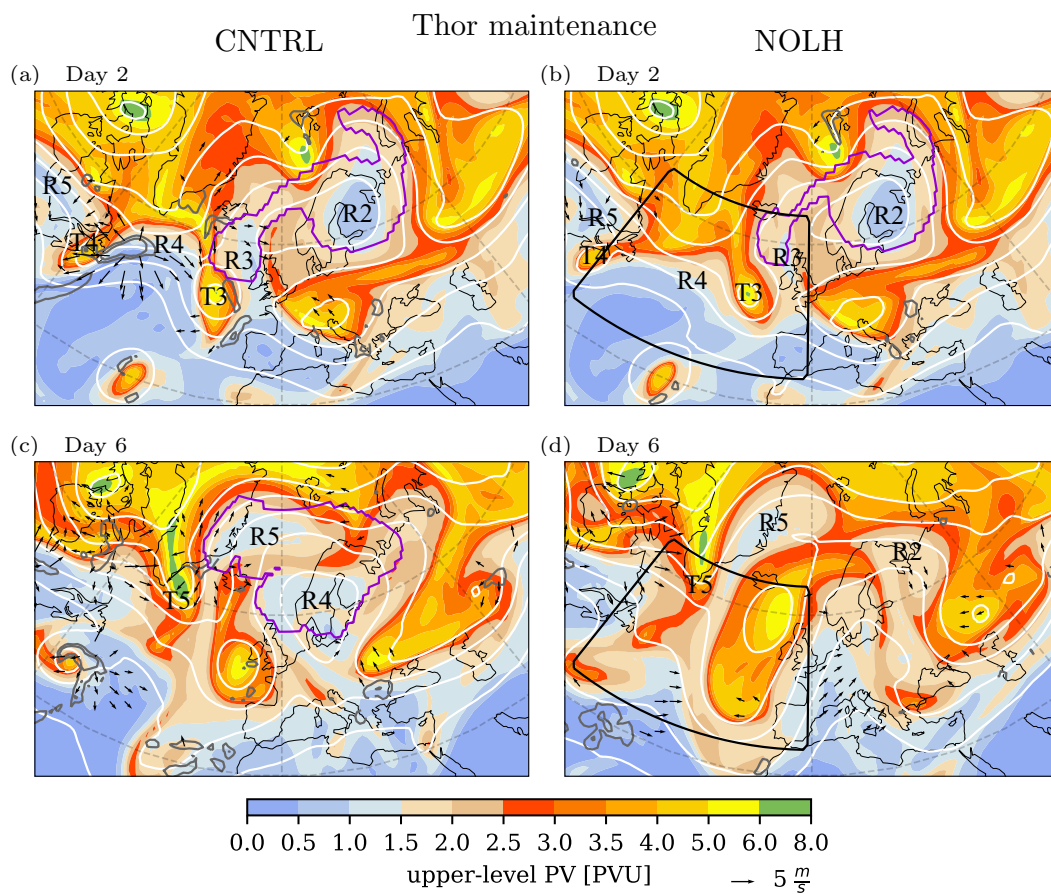


Figure 4. Same as Fig. 3, but at (a,b) 9 UTC 11 October 2016 (day 2) and (c,d) 9 UTC 16 October 2016 (day 6).

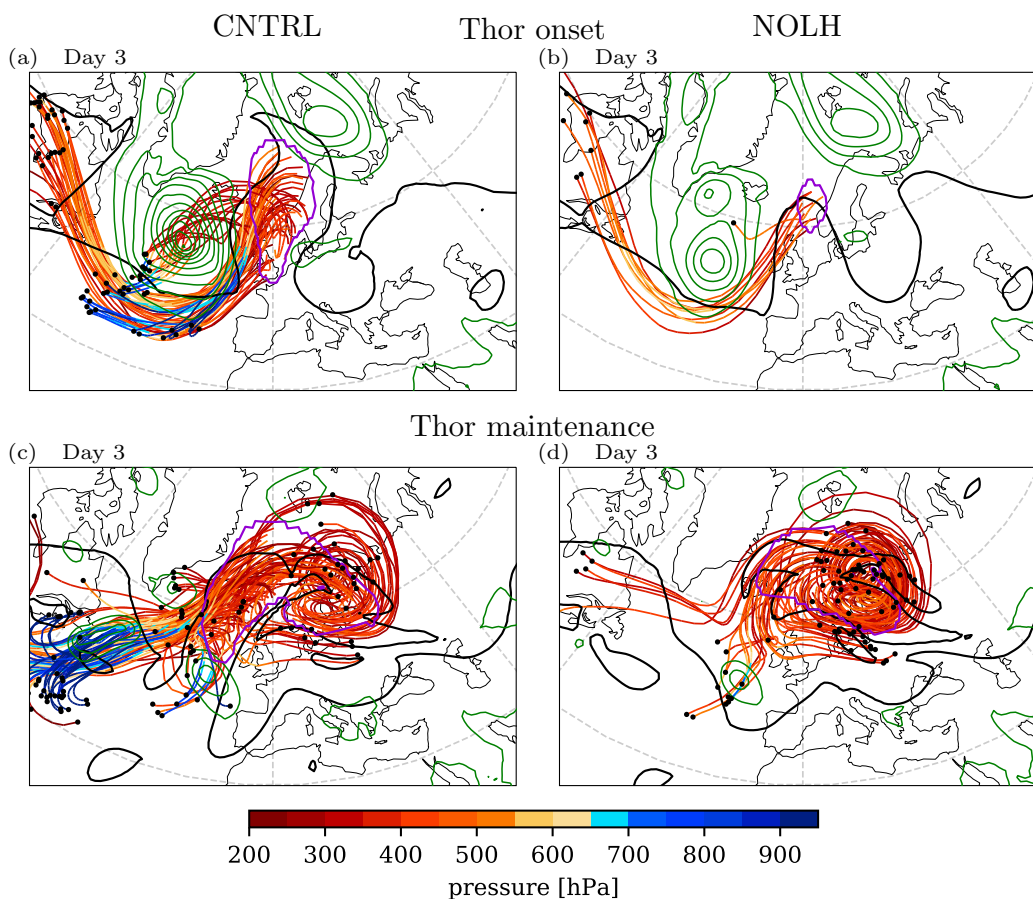


Figure 5. Upper-level 2 pvu contour (black line), SLP (green contours, from 1000 hPa every -10 hPa) and blocking region (magenta contour for upper-level PV anomaly of -1 pvu) for (a,c) CNTRL and (b,d) NOLH simulation for case Thor onset (upper panel) and Thor maintenance (lower panel). 72-h backward trajectories started in the blocking region at 00 UTC 4 October 2016 in the onset simulations and at 00 UTC 13 October 2016 in the maintenance simulations are shown as colored lines, with color indicating pressure (hPa). The black circles show the location of the backward trajectories 3 days prior to arrival in the blocking.

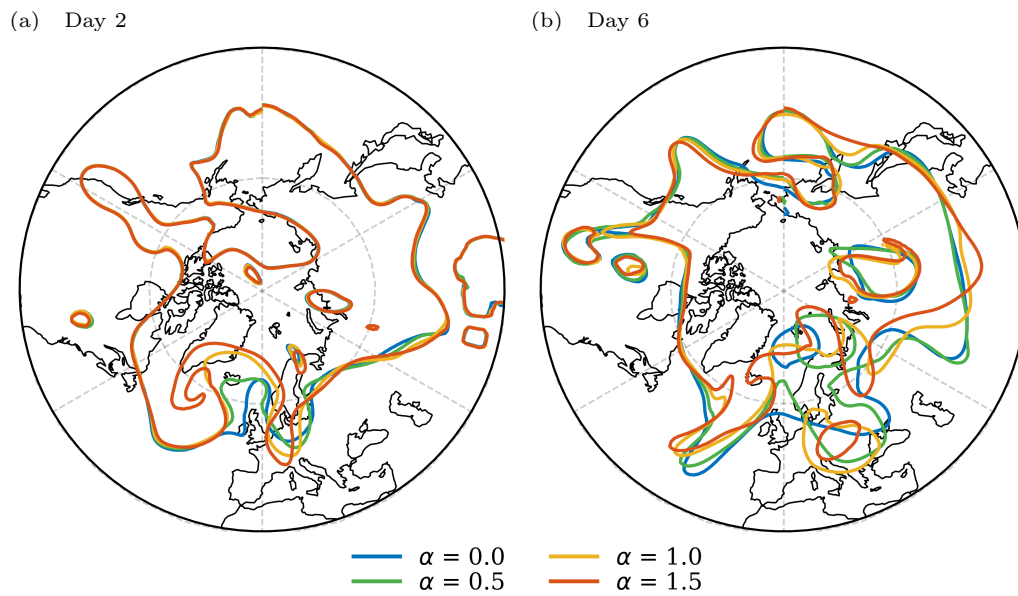


Figure 6. Dynamical tropopause (upper-level 2 pvu contour) for Thor onset during (a) 2 October 2016 (day 2) and (b) 6 October 2016 (day 6) for different α values (blue for $\alpha = 0$ (NOLH), green for $\alpha = 0.5$, yellow for $\alpha = 1$ (CNTRL), and red for $\alpha = 1.5$).

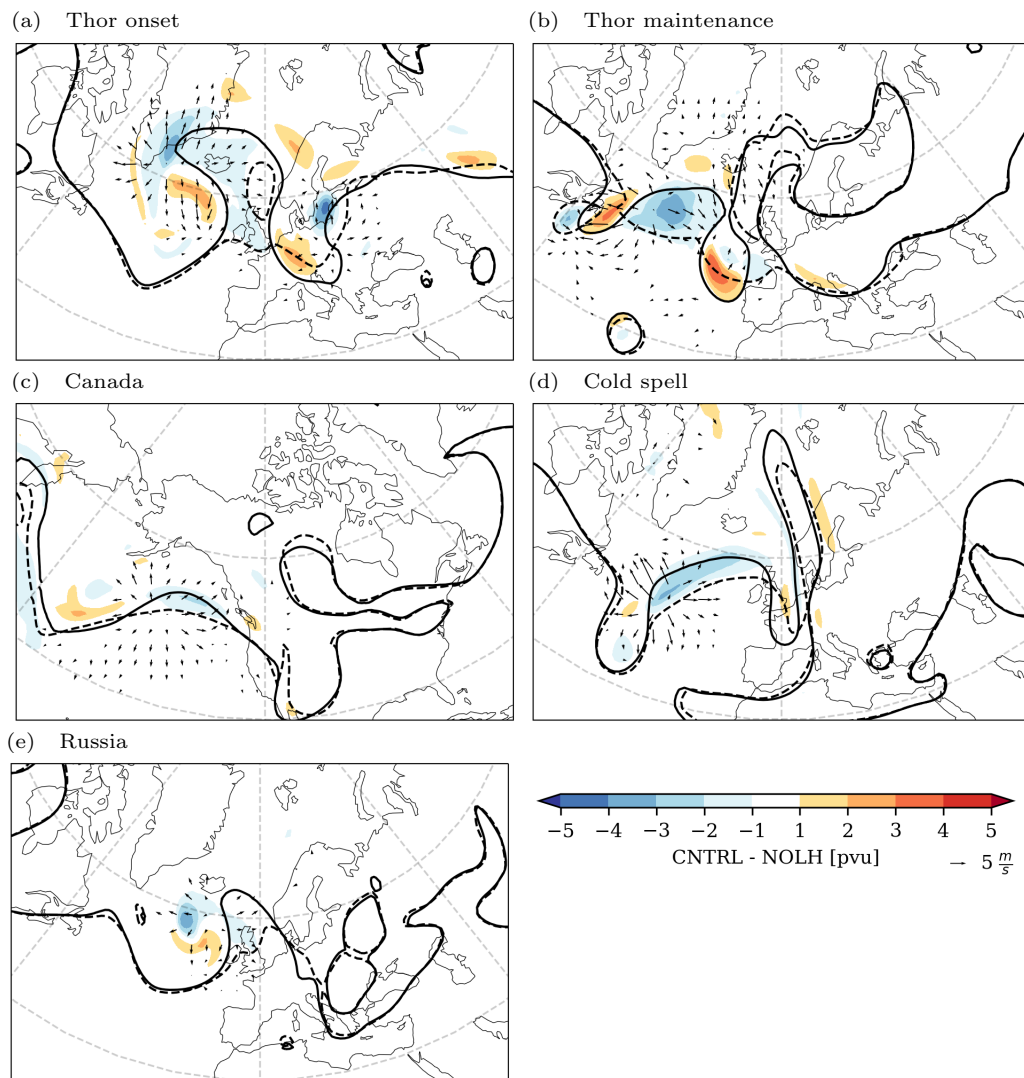


Figure 7. Difference (CNTRL - NOLH) in upper-level PV (shaded in pvu), difference in upper-level divergent wind (vectors only shown for wind speed larger than 1 m s^{-1}), and upper-level 2 pvu contour (solid for CNTRL, dashed for NOLH) after 3 days model simulation for (a) Thor onset, (b) Thor maintenance, (c) Canada, (d) Cold Spell, and (e) Russia.

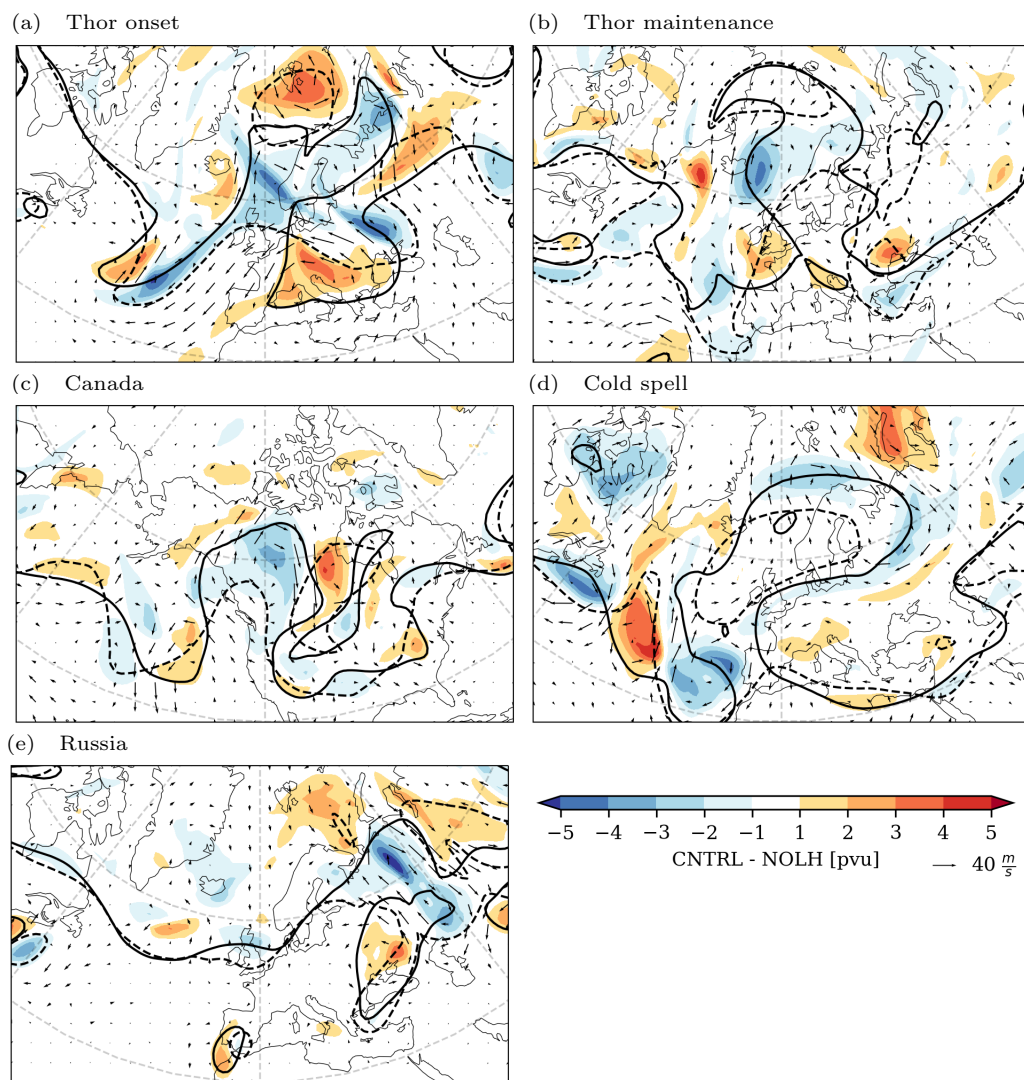


Figure 8. Difference (CNTRL - NOLH) in upper-level PV (shaded in pvu), difference in upper-level rotational wind (vectors only shown for differences larger than 1 m s^{-1}), and upper-level 2 pvu contour (solid for CNTRL, dashed for NOLH) after 6 days model simulation for (a) Thor onset, (b) Thor maintenance, (c) Canada, (d) Cold spell, and (e) Russia.

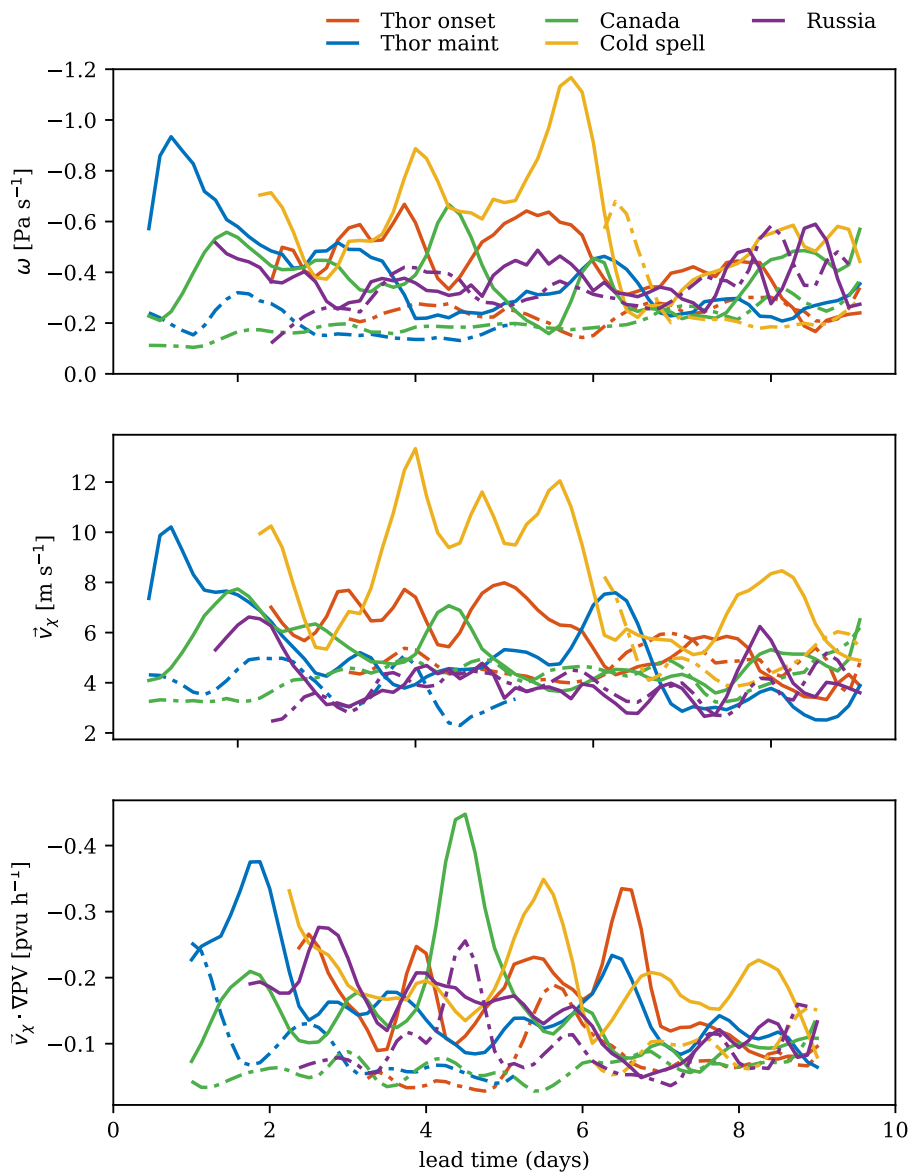


Figure 9. a) Vertical wind ω (Pa s^{-1}), (b) magnitude of divergent wind v_χ (m s^{-1}) and (c) PV advection by the divergent wind $v_\chi \cdot \nabla \text{PV}$ (pvu h^{-1}) as a function of simulation lead time. Values are averaged over a nine-grid-point box in the upper-level on the western flank of the block centered around the strongest wind/PV advection magnitudes. Solid lines for CNTRL simulations, dashed lines for NOLH simulations. Note that the individual curves start as soon as a block is identified with the APV index.

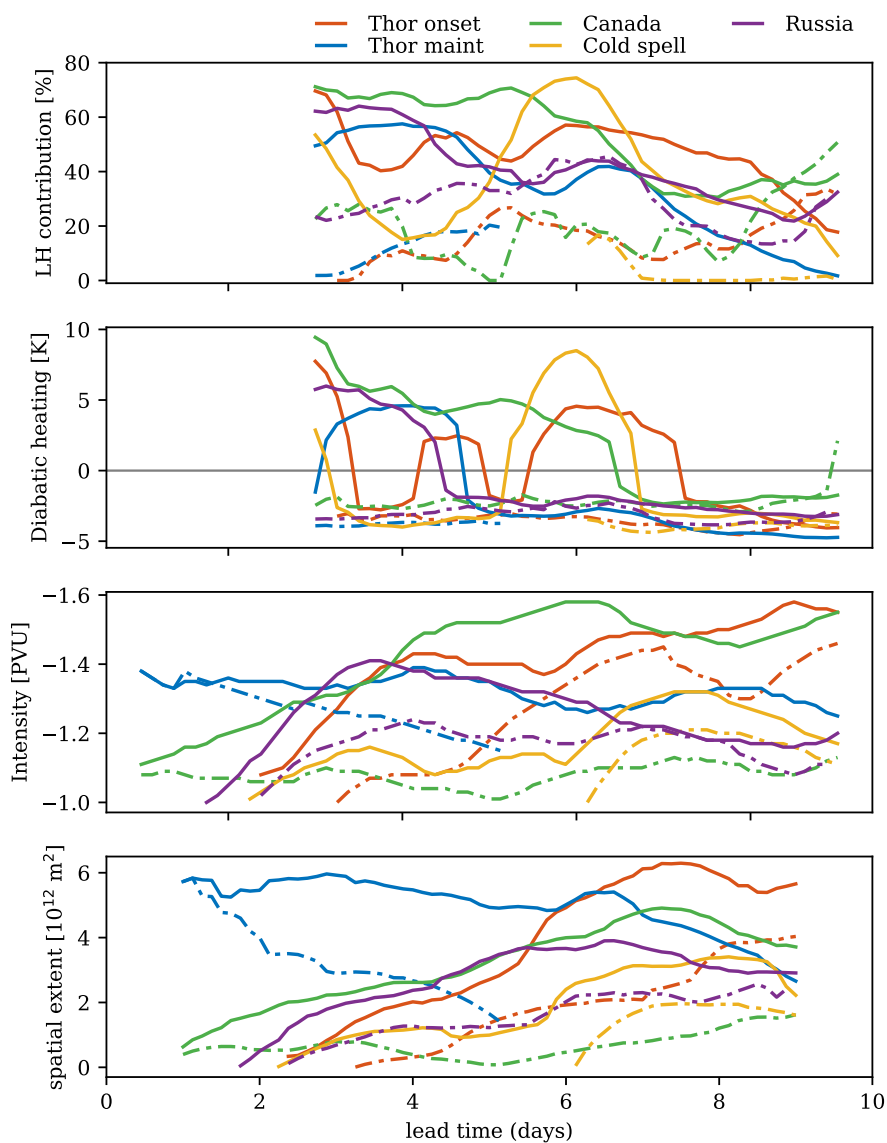


Figure 10. (a) Percentage of blocking trajectories with $\Delta\theta > 2 \text{ K}$ in 3 days (%), (b) mean diabatic heating (K), (c) blocking intensity (PV anomaly), (d) spatial extent (10^{12} m^2) as a function of simulation lead time. Solid lines for CNTRL simulations, dashed lines for NOLH simulations. Note that 3-day backward trajectories can only be calculated after day 3.



Table 1. Selected historical blocking events. The LH contribution has been determined from backward trajectory calculations. The initialization time is the same for both CNTRL and NOLH simulations. Note that "Thor onset" and "Thor maintenance" are different phases of the same blocking event.

Experiment	Initiation time	Region	NOLH box	LH contribution	
				CNTRL	NOLH
Thor onset	30 Sep 2016	Atlantic-Europe	[60°W - 0°, 35°N - 65°N]	47 %	16 %
Thor maintenance	10 Oct 2016	Atlantic-Europe	[60°W - 0°, 35°N - 65°N]	34 %	12 %
Canada	27 Apr 2016	Pacific-America	[180°W - 120°W, 35°N - 65°N]	52 %	20 %
Cold spell	18 Feb 2018	Atlantic-Europe	[60°W - 0°, 35°N - 65°N]	38 %	3 %
Russia	29 June 2010	Western Russia	[60°W - 0°, 35°N - 65°N]	42%	29%